RESEARCH ARTICLE
doi: 10.2306/scienceasia1513-1874.2024.016

ScienceAsia 50 (1): 2024: ID 2024016: **1–9**

CD142 inhibits BCL2-dependent autophagic cell death and apoptosis in Wilms' tumor

Linshan Zeng[a], **Qiang Zeng**[b], **Haifeng Zhang**[c], **Mingfeng Xie**[a], **Xiaojun Zhang**[d,*]

[a] Department of Pediatric Surgery, The First Affiliated Hospital of Gannan Medical University, Ganzhou 341000 China
[b] Department of Pediatric Surgery, Jiangxi Maternal and Child Health Hospital, Nanchang 330000 China
[c] Department of Urology, The First People's Hospital of Jiujiang City, Jiujiang 332000 China
[d] Department of Medical Oncology, The First Affiliated Hospital of Gannan Medical University, Ganzhou 341000 China

*Corresponding author, e-mail: ZXJgnyxy@163.com

Received 21 Oct 2022, Accepted 18 Aug 2023
Available online 25 Feb 2024

ABSTRACT: It is known that cluster of differentiation 142 (CD142) is closely related to the tumorigenesis of Wilms' tumor (WT). However, the underlying mechanism of CD142-regulated WT tumorigenesis remains unknown. CD142 can upregulate the expression of autophagy and apoptosis-inhibiting factor B-cell lymphoma-2 (BCL2). This study aimed to investigate whether CD142 regulates the WT tumorigenesis through the inhibition of BCL2-dependent autophagic cell death and apoptosis. Our results showed that CD142-positive sorting WT cell line WiT49 had stronger survival capacity and migratory function, while CD142-negative WiT49 cells were contrary. Moreover, xenogeneic tumor experiments showed that nude mice with $CD142^+$ WiT49 cells had stronger tumorigenicity *in vivo*. Importantly, $CD142^+$ WiT49 cells had higher protein level of BCL2, weaker autophagy, weaker apoptosis, and more significant interaction of BCL2 with Beclin1 and BAX; whereas $CD142^-$ WiT49 cells showed the opposite effects. However, BCL2 inhibition with ABT-737 intervention rescued the inhibited autophagy and apoptosis and promoted the survival and migratory function in $CD142^+$ WiT49 cells. Overall, this study demonstrated that CD142 inhibits the autophagic death and apoptosis by the overexpressed BCL2, which enhances the tumorigenesis of WT.

KEYWORDS: CD142, BCL2, autophagy, apoptosis, Wilms' tumor

INTRODUCTION

Wilms' tumor (WT) is a common malignant embryonal tumor of the kidney, accounting for 6% of the whole malignant tumors in children [1]. WT was first identified by Max Wilms in 1899 [2]. After decades of research and development on treatment, the prognosis of patients with WT has been greatly improved. With multidisciplinary (surgery, radiotherapy and chemotherapy) and individualized treatments, the overall survival rate of WT is approximately 90%. However, the prognosis is still poor in some WT patients due to recurrence, metastasis, and so on [3–5]. Furthermore, the existing treatments can result in serious side effects including musculoskeletal complications, cardiotoxicity, renal insufficiency, reproductive problems, and a second malignant neoplasm [6]. Therefore, in-depth study of the key regulatory molecules in the development of WT is of great significance for optimizing the diagnosis and treatment of the tumour and improving the prognosis of WT patients.

As a cell surface biomarker, CD142 (also known as tissue factor, TF or F3) is closely related to the tumorigenesis of multiple malignant tumors [7–10]. Firstly, CD142 is expressed in many types of tumors and used as an independent risk factor to predict the prognosis of patients with malignancies [11–14]. *In vitro* studies also showed that CD142 can promote the mobility of cancer cells [15–17]. Importantly, the positive expression of CD142 can be found in the WT tissues, and overexpressed CD142 is a critical risk factor for recurrence and mortality of WT patients [11]. However, the potential significance of CD142-regulated WT tumorigenesis is still unclear.

Apoptosis is the most common programmed death. Autophagy, as a highly conserved cellular mechanism, degrades damaged or aged organelles, decomposes unnecessary macromolecules or pathogens, releases nutrients and energy, and then maintains cell viability. Autophagy is termed as protective autophagy due to its cytoprotective effect. However, overloaded autophagy can result in cell death, i.e., autophagic cell death, which is the most common form of death besides apoptosis. Both autophagic cell death and apoptosis are the significant suppressive factors for many malignant tumors. CD142 is known to upregulate the expression of BCL2 [18, 19]. Of note, BCL2 can inhibit apoptotic signal transduction by binding pro-apoptotic molecule, Bax [20]. Furthermore, BCL2 can also suppress autophagy activation by binding autophagy molecule, Beclin1, and preventing Beclin1 from entering autophagy flux [21]. BCL2-Beclin1-autophagy signal transduction is a pivotal mechanism for driving autophagic cell death, which is reflected in the repression of a variety of malignancies [22–24].

Thus, we speculate that CD142 could promote the WT tumorigenesis by upregulating BCL2 expression and then inhibiting apoptosis and autophagic death.

Our study aimed to investigate the roles of CD142 in the tumorigenicity, BCL2 protein level and interactions, autophagy and apoptosis of WT *in vitro* and *in vivo* by fluorescence activated cell sorting (FACS). Finally, combined with the pharmacological inhibition of BCL2, the significance of BCL2 in CD142-regulated autophagy, apoptosis and tumorigenesis of WT was further explored by rescue assays.

MATERIALS AND METHODS

Cell culture

Human WT cell lines WT-CLS1, WiT49, and normal renal tubular epithelial cell line HK-2 were purchased from the American Type Culture Collection (ATCC, Manassas, USA). The cell lines have been authenticated using STR profiling. Cells were incubated in Dulbecco's modified eagle medium (DMEM; ThermoFisher Scientific, Waltham, USA) supplemented with 10% Fetal Bovine Serum (FBS; GIBCO, Grand Island, USA), and kept under 37 °C and 5% CO_2. In all *in vitro* functional experiments, WT cell lines were treated with corresponding ligand FVIIa (10 nM in all experiments).

Application of flow cytometry in sorting $CD142^+$ and $CD142^-$ cells

With the help of Fc receptor blocking solution (Human TruStain FCX receptor, BioLegend, San Diego, USA), cells (5×10^5/tube) were pretreated for 15 min at room temperature to block non-specific binding. The cells were stained using APC anti-human CD142 antibody (BioLegend) and collected on MoFlo-XDP flow cytometry (Beckman Coulter, Breya, USA). The antibody was mixed with Dulbecco's Phosphate-Buffered Saline (DPBS; GIBCO; without calcium and magnesium ions) containing 0.1% bovine serum albumin (BSA; GIBCO) to make 30 μl reaction system, and incubated on ice for 15 min. Before starting the machine, cells were resuspended by adding complete DMEM (containing 10% DFBS) to make the 300 μl liquid volume. The cells were transferred to the flow tube and detected by flow cytometry. During sorting process, the success rate of cell sorting was stable at about 80% (shown by flow cytometry). The harvested cells were $CD142^+$ cells, and the remaining cells in the flow tube were $CD142^-$ cells. These two types of cells were further cultured. The sorting efficiency was identified using Western Blot.

Western blot analysis

The indicated cells were lysed in lysis buffer containing 1% Triton X-100 and centrifuged. 10% Sodium dodecyl sulfate polyacrylamide gel electrophoresis (SDS-PAGE; ThermoFisher Scientific) gel was used to dissolve the supernatant (soluble fraction), while the particles (insoluble fraction) were suspended in the boiling SDS-PAGE loading buffer and ultrasonically treated to dissolve the protein. Next, proteins were transferred onto polyvinylidene difluoride (PVDF; Millipore, Boston, USA) membrane, followed by incubating with the antibodies targeting rabbit CD142 (#97438), LC3 (#2775), PARP (#9532), BCL2 (#15071), Beclin1 (#4122), Bax (#5023), and GAPDH (Cell Signaling Technology, Boston, USA) dissolved in 5% bovine serum albumin overnight at room temperature. Ultimately, the membranes were incubated with Horseradish peroxidase (HRP)-conjugated secondary antibodies (Cell Signaling Technology) for 1 h at room temperature. The bands were analyzed using Chemiluminescence System (Amersham Image 600, General Electric, Boston, USA).

Detection of apoptosis

The apoptosis level was assessed through Annexin V-FITC/PI staining. After the specific treatment in the experimental design, the indicated cells were collected, and then staining was performed according to manufacturer's protocols. Next, the apoptotic cells were measured and quantitatively analyzed using the flow cytometer (BD Accuri C6 Plus, BD Biosciences, USA). The apoptosis was also evaluated by measuring Caspase3 activity using ApoAlert Caspase fluorescent assay kit (Clontech, San Francisco, USA). The cells on 6-well plates were treated with the given treatments, lysed in 120 μl lysis buffers, and incubated on ice for 10 min. 120 μl reaction buffer containing 12 μl Caspase3 fluorescent substrate (1 mM) was added to each well and incubated for 1 h at 37 °C. The fluorescent intensity was quantified with a fluorospectrophotometer (Synergy2, BioTek, Vermon, USA; excitation at 400 nm and emission at 505 nm). The cells treated by Caspase3 inhibitor (DEVD-CHO, MedChemExpress, New Jersey, USA) were applied as a negative control to exclude the nonspecific hydrolysis of the substrate.

Trypan blue exclusion assays

Total death level of indicated cells was assessed via trypan blue staining. The treated cells were suspended, and 0.4% trypan blue solution (Solarbio, Beijing, China) was added at a volume ratio of 9:1. Subsequently, corresponding cells were quantified by an optical microscope. Cells failing to exclude dyes were considered dead cells. The total death rate = number of dead cells/number of total cells.

Cell proliferation assays

Cell proliferation was assessed using cell counting kit-8 (CCK-8; Dojindo, Shanghai, China). Cells were cultured in 96-well plates at a density of 2500 cells/well, and then received different treatments. Subsequently, CCK-8 reagents were added into each well, and then cells were incubated in the darkness condition for 1 h.

Ultimately, the optical density at 450 nm (OD450) was measured by using Varioskan Flash reader (ThermoFisher Scientific).

Co-immunoprecipitation (Co-IP) assays

Total protein was extracted by RIPA lysis and extraction Buffer (89900, Thermol Fisher Scientific, USA). Next, we cleaned the beads using 100 µl ice buffer, added 100 µl antibody-bound buffer, revolved the antibody and magnetic beads for 30 min, and rinsed the beads 3 times, each with 200 µl buffer for 5 min. Cell lysates and antibody-bound magnetic beads were incubated for 1 h at room temperature and cleaned using 200 µl buffers for 5 min each time. The beads were rinsed once using 20 µl elution buffer to remove the supernatant. The cell lysates were extracted for Co-IP using anti-Beclin1 antibody (Cell Signaling Technology), and then Western Blot with anti-BCL2 antibody was used to examine the precipitates.

Transmission Electron Microscope (TEM) analyses

The preparation of cell sections, staining, and TEM analysis were performed according to manufacturer's protocols (Servicebio, Wuhan, China). Then, the stained sections were observed using the Hitachi 7700 transmission electron microscope (Tokyo, Japan). The formation of autolysosomes was evaluated by counting the number of autolysosomes in corresponding cells (45 cells from 3 independent assays).

Cell migration assays

Cell migration was measured using Transwell assays. Treated cells suspended in serum-free DMEM were seeded onto the upper chamber of a Transwell (24-well insert, Millipore, Billerica, USA). DMEM containing 20% fetal bovine serum was added to the lower chamber. After 36 h of incubation, the cells migrating into lower surface of the inserts were fixed, stained with 1% crystal violet, and photographed. The migration level was measured by counting the number of stained cells.

Animal experiments

4∼6-week-old male athymic BALB/c nude mice were obtained from the Animal center of Gem Pharmatech Co., Ltd. (Nanjing, China). The corresponding cells were inoculated subcutaneously on the ventral side of the right rib at the density of 4×10^6 cells per mouse (8 mice/group). The volumes of xenografts in each group of mice were measured every three days to observe the tumor growth. The shortest diameter (A) and the longest diameter (B) were measured with a caliper to determine the xenograft volume. The volume (V) was calculated using the formula $V = (A^2 \times B)/2$. After 30 days, tumor-bearing mice were sacrificed via cervical dislocation under anesthesia with thiopental (15 mg/kg), and all tumors were removed and weighed. The sacrifice of mice was confirmed when the heart and breathing stopped. These experimental protocols were approved by the Institutional Animal Care and Use Committee of First Affiliated Hospital of Gannan Medical University (Gannan, China). All mice were housed in a specific pathogen-free facility with barrier, the room temperature at 20∼30 °C, and the humidity 60∼80%. The mice were fed a SPF mouse chow and sterile water.

Statistical analysis

Statistical analyses were performed using SPSS19.0. The data were presented as mean ± SEM. For comparisons, Student's *t*-test, one-way ANOVA analysis, and two-way ANOVA analysis were carried out. Bonferroni test was used for Post-Hoc multiple comparisons of one-way or two-way ANOVA. $p < 0.05$ indicated significant difference.

RESULTS

$CD142^+$ WT cells had stronger survival and migration ability

We first investigated the expression of CD142 in WT cell lines and renal epithelial cell line. It was observed that CD142 protein expression was significantly increased in WT cell lines WiT49 and WT-CLS1 compared with renal epithelial cell line HK-2 (Fig. 1A). Then, we sorted $CD142^+$ and $CD142^-$ WiT49 cells by FACS assays. The cell sorting efficiency was verified using Western Blot assay (Fig. 1B). As shown in Fig. 1B, $CD142^+$ WiT49 cells showed a higher level of proliferation than $CD142^-$ or control cells (Fig. 1C). Moreover, the proliferation level of $CD142^-$ WiT49 cells was significantly lower than that of control cells (Fig. 1C). In addition, compared with $CD142^-$ or control WiT49 cells, $CD142^+$ cells showed lower total death level (Fig. 1D). Moreover, the total death level of $CD142^-$ WiT49 cells was significantly higher than those of control cells (Fig. 1D). Remarkably, $CD142^+$ WiT49 cells showed a higher migration level than $CD142^-$ or control cells (Fig. 1E-F). Furthermore, the migration level of $CD142^-$ WiT49 cells was significantly lower than that of control cells (Fig. 1E-F).

Nude mice with $CD142^+$ WT cells had stronger tumorigenicity *in vivo*

The *in vitro* effect of CD142 on WT cells has been elucidated. The *in vivo* effect of CD142 on WT needs to be further clarified. We inoculated $CD142^+$, $CD142^-$, and control WiT49 cells into nude mice. The *in vivo* inoculation efficiency of the above cells was verified by Western Blot assay (Fig. 2D-E). As shown in Fig. 2B, compared with the tumors in the nude mice inoculated with $CD142^-$ or control cells, those of the nude mice inoculated with $CD142^+$ cells had greater size and weight (Fig. 2A-B). In addition, the nude mice inoculated with $CD142^-$ cells had smaller size and weight

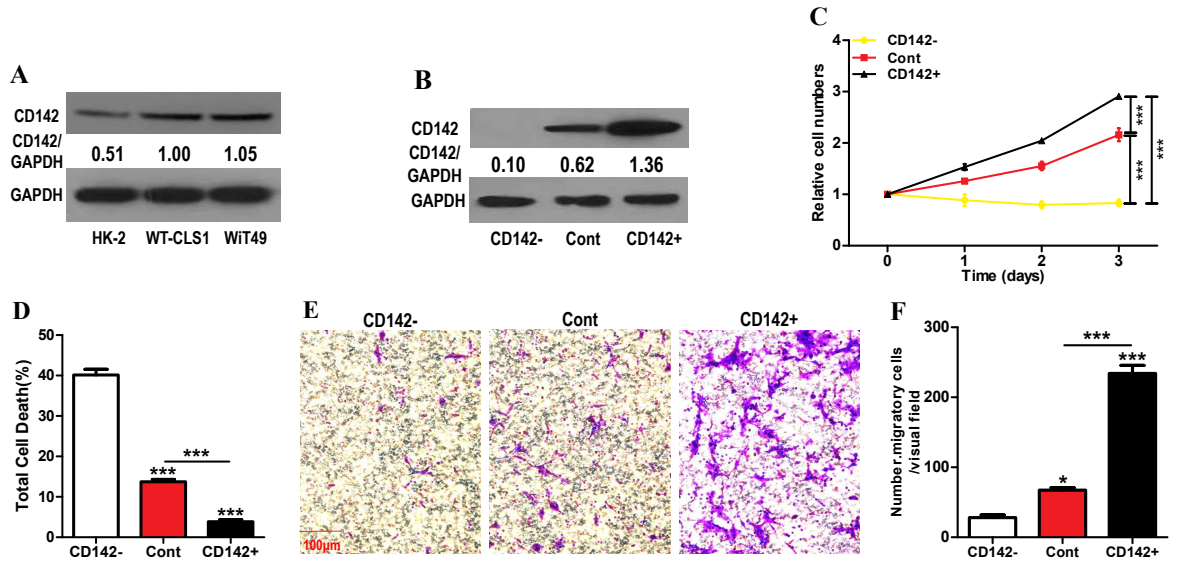

Fig. 1 Stronger survival and migration ability in CD142$^+$ WT cells. (A), CD142 protein expression in human WT cell lines WT-CLS1, WiT49 and normal renal tubular epithelial cell line HK-2; (B), CD142 protein expression in CD142$^-$, CD142$^+$ WiT49 cells by fluorescence activated cell sorting and control cells; (C), Corresponding cell proliferation assessed by CCK-8 assays; (D), Total death level of corresponding cells incubated for 24 h measured by trypan blue staining; (E), Corresponding cell migration assessed by Transwell assays. Scale bar, 100 μm; (F), The histogram representing migratory cell number in each group in F. Results are expressed as mean ± SEM from three independent experiments. * $p < 0.05$, *** $p < 0.001$ by one-way ANOVA test and Bonferroni Post-Hoc multiple comparisons. Cont, control group.

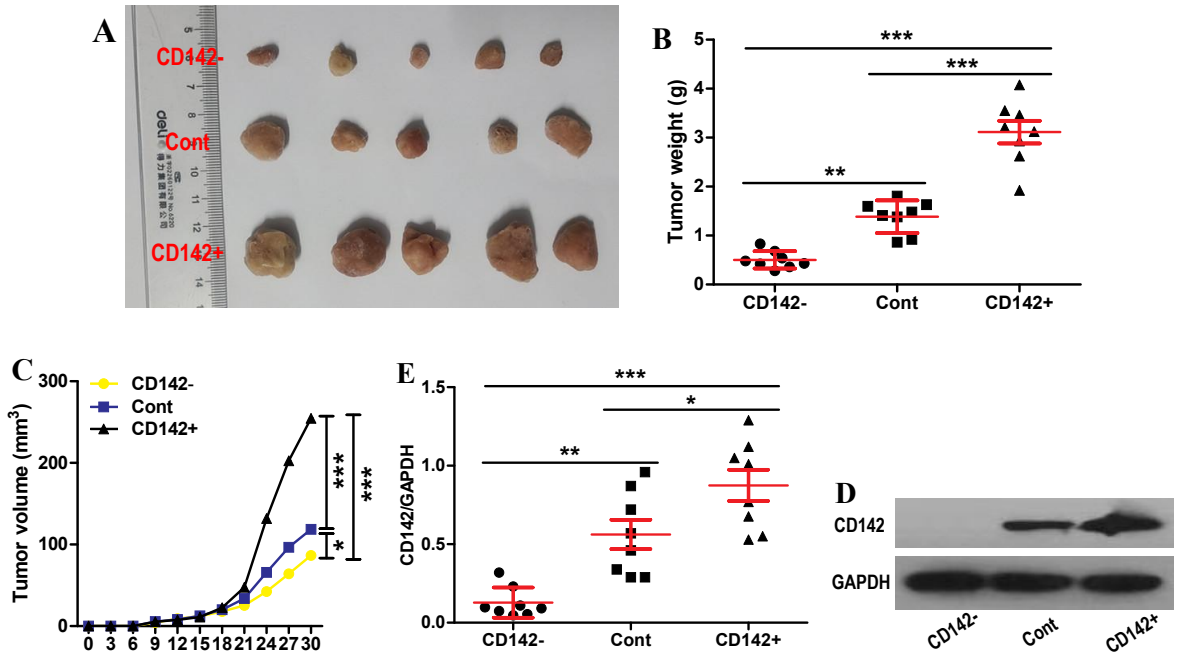

Fig. 2 Stronger tumorigenicity *in vivo* in Nude mice with CD142$^+$ WT cells. Different sorting cells were inoculated into nude mice. 30 days later, the whole mice were killed, and tumors were removed and weighed. (A), Representative images of the removed tumors from each group; (B), The histogram representing the weights of the removed tumors ($n = 8$); (C), Statistical graph displaying the growth curves of tumor volumes from each group ($n = 8$); (D-E), CD142 protein expression of tumor tissues from each group ($n = 8$). Results are expressed as mean ± SEM. * $p < 0.05$, ** $p < 0.01$, *** $p < 0.001$ by one-way ANOVA test and Bonferroni Post-Hoc multiple comparisons. Cont, control group.

of tumors than control WiT49 cells (Fig. 2A-B). Consistently, nude mice inoculated with $CD142^+$ cells had a higher tumor growth curve than nude mice inoculated with $CD142^-$ or control cells (Fig. 2C). Moreover, nude mice inoculated with $CD142^-$ cells had a lower tumor growth curve than control cells (Fig. 2C).

$CD142^+$ WT cells had lower autophagy activity and apoptosis level

CD142 is known to promote BCL2 expression [18, 19]. Accordingly, we further investigated the effects of CD142 on BCL2 protein level, autophagy activity, and apoptosis level in WT cells. Compared with $CD142^-$ or control WiT49 cells, $CD142^+$ cells showed a stronger BCL2 protein expression and a weaker LC3 transformation rate (LC3II/I) and cleaved-PARP expression (Fig. 3A). In addition, $CD142^-$ WiT49 cells had a lower BCL2 protein expression than control cells, but a higher LC3 transformation and cleaved-PARP expression (Fig. 3A). Similarly, the number of autolysosomes in $CD142^+$ WiT49 cells increased significantly compared with that of $CD142^-$ or control cells (Fig. 3B-C). Moreover, $CD142^-$ WiT49 cells had more autolysosomes than control cells (Fig. 3B-C). Apoptotic cells observed by Annexin V-FITC/PI staining showed a similar trend to the number of autolysosomes (Fig. 3D-E). The above results indicated that CD142 promoted BCL2 expression and inhibited autophagy activity and apoptosis level in WT cells. The significance of CD142 in BCL2-Beclin1/Bax complexes of WT cells is also worthy of further exploration. As shown in Fig. 3F, the co-immunoprecipitation capacity of BCL2 and Beclin1 or Bax in $CD142^-$ WiT49 cells decreased, while the co-immunoprecipitation capacity of BCL2 and Beclin1 or Bax in $CD142^+$ cells increased, supporting that CD142 can promote the interaction between BCL2 and Beclin1 or Bax.

Treatment of ABT-737 reversed the attenuated autophagy and apoptosis in $CD142^+$ WT cells

We documented that CD142 can promote BCL2 protein expression and inhibit the autophagy and apoptosis in WT cells. The roles of BCL2 in CD142-regulated autophagy activity and apoptosis level in WT cells should also be further explored. As shown in Fig. 4A, compared with control WiT49 cells, $CD142^+$ cells had weaker LC3 transformation and cleaved-PARP expression, which was reversed by BCL2 inhibitor, ABT-737. We used chloroquine, an autophagy flux blocker, to verify the fluency of autophagy flux in our experimental system. As shown in Fig. 4B, the addition of chloroquine increased the LC3 transformation of $CD142^-$, $CD142^+$ and control WiT49 cells; and LC3 transformation showed a similar trend to that of Fig. 3A in the absence or presence of chloroquine, which proved the reliability of our experimental system. In addition, the detection of p62 showed that in the presence or absence of chloroquine, p62 protein level increased with the increase of CD142 expression in the three groups. Moreover, p62 expression level in chloroquine groups was higher than that in non-chloroquine groups. Combined with the detection results of LC3 and p62, we believed that under chloroquine intervention, although the LC3 transformation in $CD142^-$ cells is the highest, considering the strongest BCL2-dependent autophagy and the lowest p62 level, CD142 plays an inhibitory role in the autophagy activity in WT cells, including autophagy flux.

In addition, compared with control WiT49 cells, $CD142^+$ cells had lower level of Caspase3 activity and total death, which was recovered by ABT-737 administration (Fig. 4C-D). Consistently, the elevated level of proliferation and migration in $CD142^+$ WiT49 cells was reversed by ABT-737 administration (Fig. 4E-G). As shown in Fig. S1A-B, treatment with 3-MA or Z-VAD promoted the proliferative capacity of $CD142^-$ and control cells, supporting the contribution of inhibition of autophagy or apoptosis to WT cell survival. Moreover, treatment with 3-MA or Z-VAD slightly increased the proliferation level of $CD142^+$ cells. However, there was no statistical difference between the two groups (Fig. S1A-B).

DISCUSSION

CD142 is known to be an important biomarker for predicting the prognosis of WT [11]. Our results also showed that WT cells had increased CD142 expression compared with renal epithelial cells. However, how CD142 regulates WT tumorigenesis is still unknown. CD142 can upregulate BCL2, and BCL2 functions as an anti-apoptotic factor and an autophagic inhibitor, which leaves an interesting scientific issue for our research, whether CD142 can inhibit autophagic cell death and apoptosis of WT by promoting BCL2 expression, thus promoting WT tumorigenesis. In order to answer the above question, we applied FACS assays targeting CD142, combined with xenotumor technology and pharmacological intervention, to explore the roles of BCL2-Beclin1-autophagy and BCL2-Bax-apoptosis signaling in CD142-regulated WT tumorigenesis. Our data revealed for the first time a novel signaling pathway related to WT tumorigenesis, CD142-BCL2-autophagy inactivation/apoptosis inhibition.

First of all, $CD142^+$ WT cells by FACS assays showed higher levels of survival and migration than control and $CD142^-$ WT cells. *In vivo* assays also showed that the inoculation of $CD142^+$ WT cells significantly enhanced the growth of xenografts in nude mice. However, compared with $CD142^-$ and control cells, $CD142^+$ WT cells had lower level of autophagy and apoptosis. Previous studies have shown that autophagy inhibition exists in clinical specimens of WT [25]. From our study, it was observed that CD142 overexpression significantly inhibited the autophagy

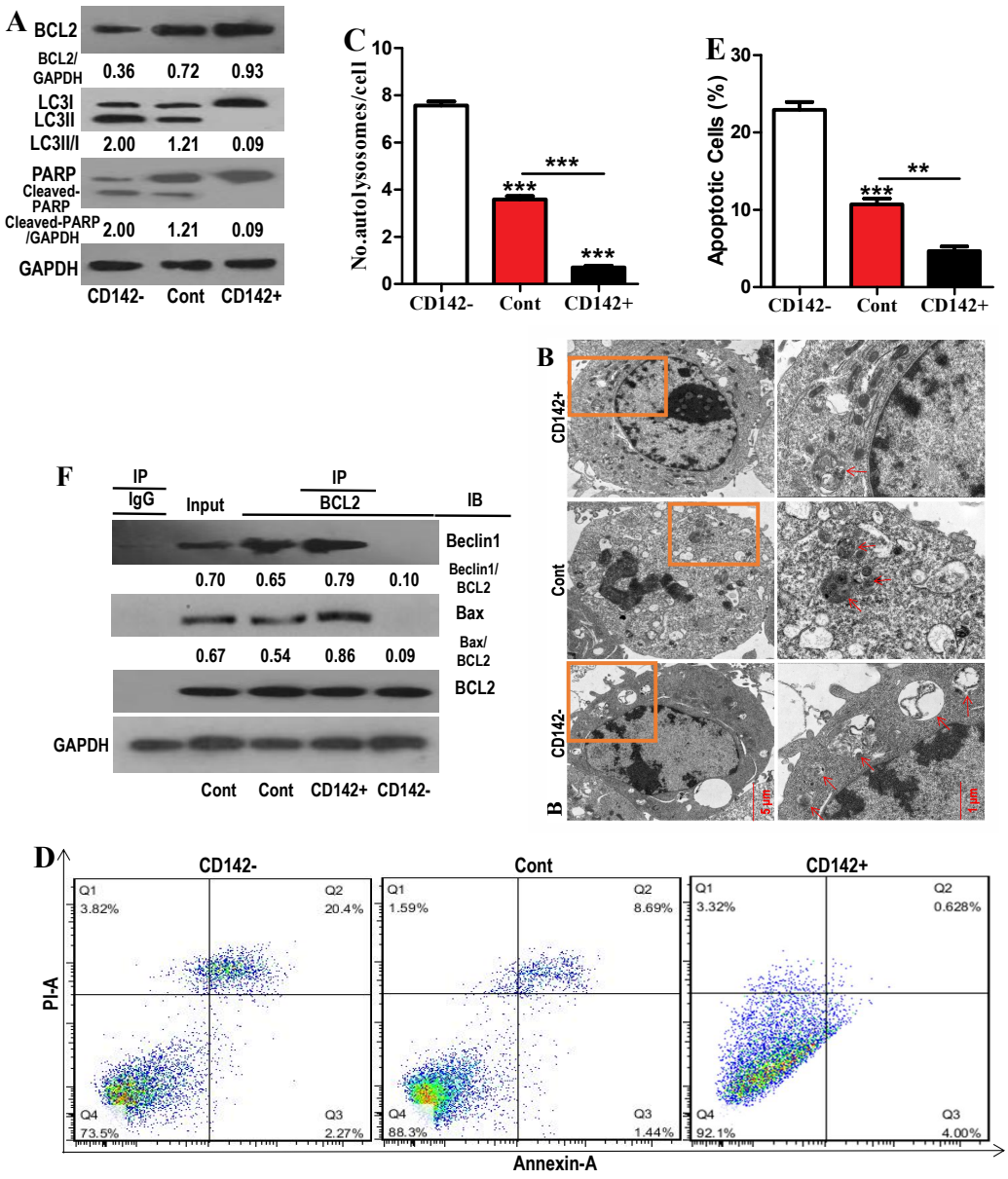

Fig. 3 Lower autophagy activity and apoptosis level in CD142$^+$ WT cells. (A), Protein expression of BCL2 and PARP and LC3 transformation in corresponding cells incubated for 12 h; (B), The formation of autolysosomes in corresponding cells incubated for 24 h (Red arrow). Scale bar, 5 or 1 μm; (C), The histogram representing autolysosome number in each group in B (60 cells from three independent assays; (D), Cell apoptosis in each group examined by flow cytometry of Annexin/PI staining; (E), The percentages of apoptotic cells (ANNEXIN-positive cells) according to the results in D; (F), Co-IP of lysates from corresponding cells incubated for 8 h and examination of precipitates. Results are expressed as mean ± SEM from three independent experiments. ** $p < 0.01$, *** $p < 0.001$ by one-way ANOVA test and Bonferroni Post-Hoc multiple comparisons. Cont, control group; IP, the antibody for immunoprecipitation; IB, the antibody for immunoblot.

responses of WT cells. Apoptosis and autophagy are known as type 1 and type 2 programmed deaths, respectively. A previous study showed that both autophagy and apoptosis are tumor suppressor pathways, and defective or inadequate levels of autophagy or apoptosis can lead to cancer [26]. Combining the above results, it was suggested that CD142 enhanced the tumorigenicity of WT through the inhibition of

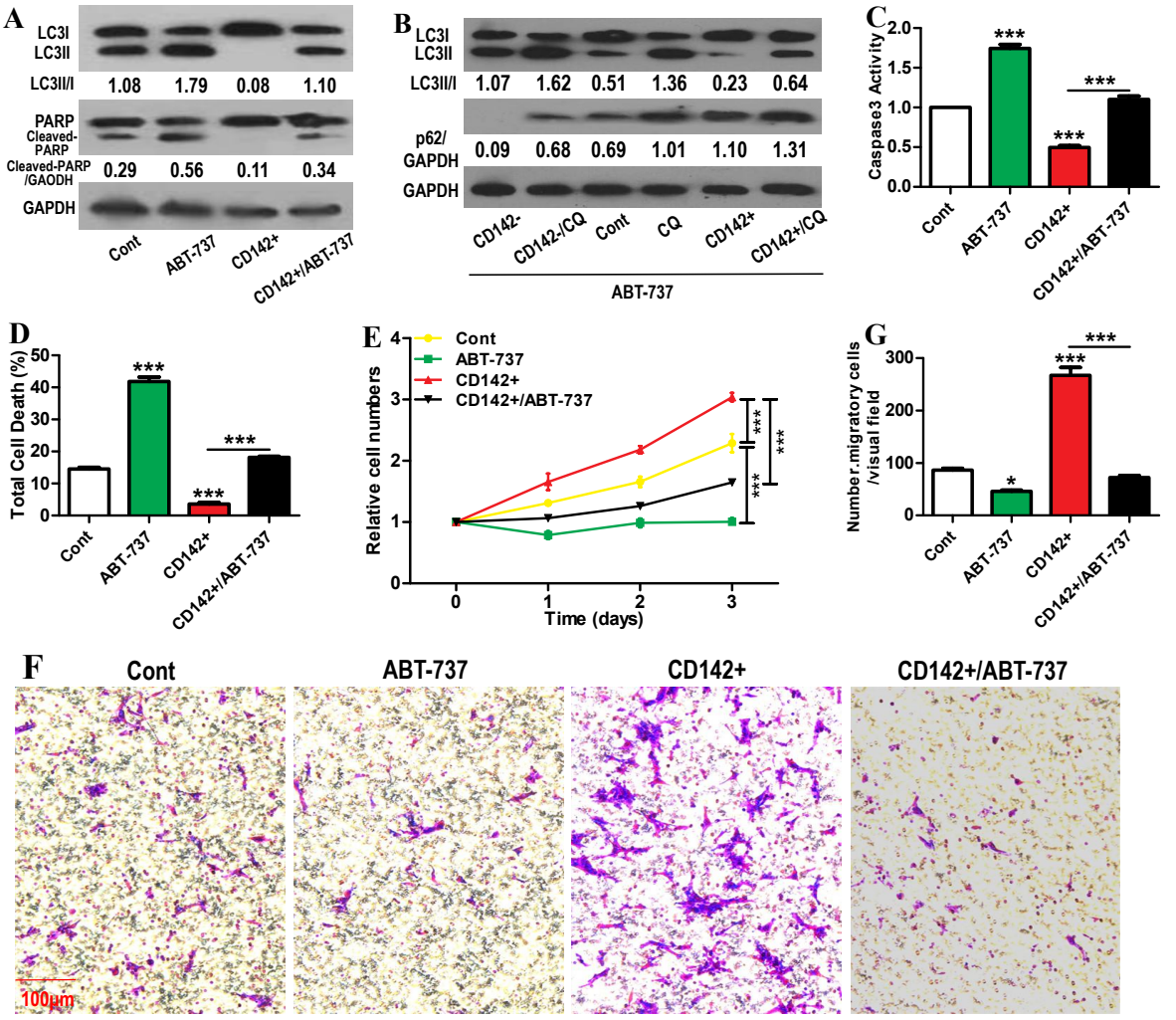

Fig. 4 Recovery of ABT-737 in attenuated autophagy and apoptosis in CD142$^+$ WT cells. (A), LC3 transformation and PARP protein expression in corresponding cells with or without ABT-737 administration (10 μM) for 12 h; (B), LC3 transformation and p62 protein expression in corresponding cells in the presence of ABT-737 for 12 h; (C), Corresponding cell apoptosis with or without ABT-737 administration for 24 h assessed by Caspase3 activity; (D), Corresponding cell death with or without ABT-737 administration for 24 h measured by trypan blue staining; (E), Corresponding cell proliferation with or without ABT-737 administration assessed by CCK-8 assays; (F), Corresponding cell migration with or without ABT-737 administration assessed by Transwell assays. Scale bar, 100 μm; (G), The histogram representing migratory cell number in each group in E. Results are expressed as mean ± SEM from three independent experiments. * $p < 0.05$, *** $p < 0.001$ by two-way ANOVA test and Bonferroni Post-Hoc multiple comparisons. Cont, control group.

apoptosis and autophagic cell death. More importantly, CD142$^+$ WT cells showed higher BCL2 expression and more significant interaction between BCL2 and Beclin1/Bax than the CD142$^-$. BCL2 molecule protects cells from programmed cell death, whose overexpression is proposed to be tumorigenic, and classical WT also expresses a large amount of BCL2 mRNA and protein [27]. Therefore, it could be inferred that CD142 promotes WT cell survival by overexpressing BCL2. Under the corresponding stress, BCL2-Beclin1 complex is dissociated, leading to Beclin1 entering autophagy flux and subsequent autophagy activation [21, 28]. The pro-apoptotic molecules including Bax can also cause subsequent apoptotic signal transduction after breaking away from the connection of BCL2 [20]. It is indicated that CD142 prevents Beclin1 or Bax from dissociating from corresponding complexes through BCL2 upregulation, which suppresses BCL2-dependent autophagy activation and apoptosis. It was also previously reported that the inhibition

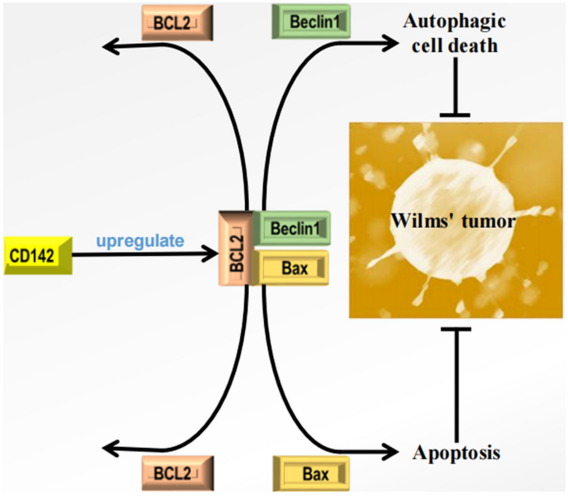

Fig. 5 The significance of BCL2-autophagy/apoptosis signaling in CD142-regulated Wilms' tumor. In brief, CD142 upregulates BCL2 protein level in WT cells, making more BCL2 bind to Bax and Beclin1 molecules, which inhibits the release of Beclin1 to autophagy flux and Bax-induced apoptotic signal transduction. Therefore, CD142 suppresses Beclin1-dependent autophagic cell death and Bax-dependent apoptosis by enhancing BCL2 expression, thereby promoting WT tumorigenesis.

of Beclin1 protein expression and the decreased autophagy activity coexist in WT tissues [25]. Therefore, our results also explain the aforementioned biological phenomena to a certain extent. Together, we elucidated the roles of BCL2-dependent autophagy and apoptosis in CD142-regulated WT tumorigenesis. The inhibited BCL2 by ABT-737 administration could recover the inhibited autophagy and apoptosis as well as enhanced survival and migration in WT caused by CD142 overexpression, which further confirmed the above conclusion. In addition, the assays based on autophagy and Caspase inhibitors indicated that inhibition of autophagy or apoptosis can promote WT cell proliferation, which is consistent with our inference. Furthermore, autophagy and Caspase inhibitors are almost ineffective on $CD142^+$ cell proliferation, which is due to BCL2 upregulation caused by CD142 positive sorting, resulting in insufficient space for autophagy or apoptosis inhibition. Remarkably, the proliferation level achieved by autophagy or Caspase inhibitor in $CD142^-$ and control cells is still lower than that of $CD142^+$ cells, indicating that inhibition of autophagy or apoptosis can only partially restore WT cell survival inhibited by insufficient CD142 level. These results further demonstrate that both autophagic death inhibition and apoptosis inhibition contribute to CD142-promoted WT tumorigenesis. Our current working model is illustrated in Fig. 5.

CONCLUSION

From the latest evidence obtained from this study, we have a deeper understanding of the underlying mechanism in CD142-regulated WT tumorigenesis, which is closely related to the two most common forms of death. We believe that WT tissues with high expression of CD142 may be more sensitive to targeted therapy against BCL2 and treatment regimens that promote autophagic cell death and apoptosis than the currently used protocols. Accordingly, this study provides more potential clues for the improvement of the diagnosis and treatment of WT.

Appendix A. Supplementary data

Supplementary data associated with this article can be found at http://dx.doi.org/10.2306/scienceasia1513-1874.2024.016.

Acknowledgements: This work was supported by Ganzhou guiding science and technology plan project (GZ2018ZSF021).

REFERENCES

1. Sung H, Ferlay J, Siegel RL, Laversanne M, Soerjomataram I, Jemal A, Bray F (2021) Global cancer statistics 2020: Globocan estimates of incidence and mortality worldwide for 36 cancers in 185 countries. *CA Cancer J Clin* **71**, 209–249.
2. Raffensperger J (2015) Max Wilms and his tumor. *J Pediatr Surg* **50**, 356–359.
3. Raval MV, Bilimoria KY, Bentrem DJ, Stewart AK, Winchester DP, Ko CY, Reynolds M (2010) Nodal evaluation in Wilms' tumors: analysis of the national cancer data base. *Ann Surg* **251**, 559–565.
4. Malogolowkin M, Cotton CA, Green DM, Breslow NE, Perlman E, Miser J, Ritchey ML, Thomas PR, et al (2008) Treatment of Wilms tumor relapsing after initial treatment with vincristine, actinomycin D, and doxorubicin. A report from the national Wilms tumor study group. *Pediatr Blood Cancer* **50**, 236–241.
5. Oue T, Koshinaga T, Takimoto T, Okita H, Tanaka Y, Nozaki M, Haruta M, Kaneko Y, et al (2016) Anaplastic histology Wilms' tumors registered to the Japan Wilms' tumor study group are less aggressive than that in the national Wilms' tumor study 5. *Pediatr Surg Int* **32**, 851–855.
6. Wright KD, Green DM, Daw NC (2009) Late effects of treatment for Wilms tumor. *Pediatr Hematol Oncol* **26**, 407–413.
7. Liu S, Zhang Y, Zhao X, Wang J, Di C, Zhao Y, Ji T, Cheng K, et al (2019) Tumor-specific silencing of tissue factor suppresses metastasis and prevents cancer-associated hypercoagulability. *Nano Lett* **19**, 4721–4730.
8. Xu C, Gui Q, Chen W, Wu L, Sun W, Zhang N, Xu Q, Wang J, et al (2011) Small interference RNA targeting tissue factor inhibits human lung adenocarcinoma growth *in vitro* and *in vivo*. *J Exp Clin Cancer Res* **30**, 63.
9. Ngo CV, Picha K, McCabe F, Millar H, Tawadros R, Tam SH, Nakada MT, Anderson GM (2007) CNTO 859, a humanized anti-tissue factor monoclonal antibody, is a potent inhibitor of breast cancer metastasis and tu-

mor growth in xenograft models. *Int J Cancer* **120**, 1261–1267.
10. Hu Z, Shen R, Campbell A, McMichael E, Yu L, Ramaswamy B, London CA, Xu T, et al (2018) Targeting tissue hactor for immunotherapy of triple-negative breast cancer using a second-generation ICON. *Cancer Immunol Res* **6**, 671–684.
11. Maciel EO, Carvalhal GF, da Silva VD, Batista EL, Garicochea B (2009) Increased tissue factor expression and poor nephroblastoma prognosis. *J Urol* **182**, 1594–1599.
12. Poon RT, Lau CP, Ho JW, Yu WC, Fan ST, Wong J (2003) Tissue factor expression correlates with tumor angiogenesis and invasiveness in human hepatocellular carcinoma. *Clin Cancer Res* **9**, 5339–5345.
13. Nitori N, Ino Y, Nakanishi Y, Yamada T, Honda K, Yanagihara K, Kosuge T, Kanai Y, et al (2005) Prognostic significance of tissue factor in pancreatic ductal adenocarcinoma. *Clin Cancer Res* **11**, 2531–2539.
14. Shigemori C, Wada H, Matsumoto K, Shiku H, Nakamura S, Suzuki H (1998) Tissue factor expression and metastatic potential of colorectal cancer. *Thromb Haemost* **80**, 894–898.
15. Chanakira A, Westmark PR, Ong IM, Sheehan JP (2017) Tissue factor-factor VIIa complex triggers protease activated receptor 2-dependent growth factor release and migration in ovarian cancer. *Gynecol Oncol* **145**, 167–175.
16. Tieken C, Verboom MC, Ruf W, Gelderblom H, Bovée JV, Reitsma PH, Cleton-Jansen AM, Versteeg HH (2016) Tissue factor associates with survival and regulates tumour progression in osteosarcoma. *Thromb Haemost* **115**, 1025–1033.
17. Xu Y, Wu D, Jiang Z, Zhang Y, Wang S, Ma Z, Hui B, Wang J, et al (2018) MiR-616-3p modulates cell proliferation and migration through targeting tissue factor pathway inhibitor 2 in preeclampsia. *Cell Prolif* **51**, e12490.
18. Wu J, Li A, Li Y, Li X, Zhang Q, Song W, Wang Y, Ogutu JO, et al (2016) Chlorpromazine inhibits mitochondrial apoptotic pathway via increasing expression of tissue factor. *Int J Biochem Cell Biol* **70**, 82–91.
19. Fang J, Gu L, Zhu N, Tang H, Alvarado CS, Zhou M (2008) Tissue factor/FVIIa activates Bcl-2 and prevents doxorubicin-induced apoptosis in neuroblastoma cells. *BMC Cancer* **88**, 69.
20. Ke D, Yu Y, Li C, Han J, Xu J (2022) Phosphorylation of BCL2 at the Ser70 site mediates RANKL-induced osteoclast precursor autophagy and osteoclastogenesis. *Mol Med* **28**, 22.
21. Pattingre S, Tassa A, Qu X, Garuti R, Liang XH, Mizushima N, Packer M, Schneider MD, et al (2005) Bcl-2 antiapoptotic proteins inhibit Beclin1-dependent autophagy. *Cell* **122**, 927–939.
22. Hseu YC, Chiang YC, Vudhya Gowrisankar Y, Lin KY, Huang ST, Shrestha S, Chang GR, Yang HL (2020) The *in vitro* and *in vivo* anticancer properties of chalcone flavokawain B through induction of ROS-mediated apoptotic and autophagic cell death in human melanoma cells. *Cancers (Basel)* **12**, 2936.
23. Wang L, Li J, Shi X, Li S, Tang PM, Li Z, Li H, Wei C (2019) Antimalarial dihydroartemisinin triggers autophagy within HeLa cells of human cervical cancer through Bcl-2 phosphorylation at ser70. *Phytomedicine* **52**, 147–156.
24. Li S, Lin Z, Zheng W, Zheng L, Chen X, Yan Z, Cheng Z, Yan H, et al (2019) IL-17A inhibits autophagic activity of HCC cells by inhibiting the degradation of Bcl2. *Biochem Biophys Res Commun* **509**, 194–200.
25. Li LJ, Wang YL, Yuan LQ, Gu WZ, Zhu K, Yang M, Zhou D, Lv Y, et al (2018) Autophagy inhibition in childhood nephroblastoma and the therapeutic significance. *Curr Cancer Drug Targets* **18**, 295–303.
26. Su M, Mei Y, Sinha S (2013) Role of the crosstalk between autophagy and apoptosis in cancer. *J Oncol* **2013**, 102735.
27. Re GG, Hazen-Martin DJ, El Bahtimi R, Brownlee NA, Willingham MC, Garvin AJ (1999) Prognostic significance of Bcl-2 in Wilms' tumor and oncogenic potential of Bcl-X(L) in rare tumor cases. *Int J Cancer* **84**, 192–200.
28. Ke D, Ji L, Wang Y, Fu X, Chen J, Wang F, Zhao D, Xue Y, et al (2019) JNK1 regulates RANKL-induced osteoclastogenesis via activation of a novel Bcl-2-Beclin1-autophagy pathway. *FASEB J* **33**, 11082–11095.

Appendix A. Supplementary data

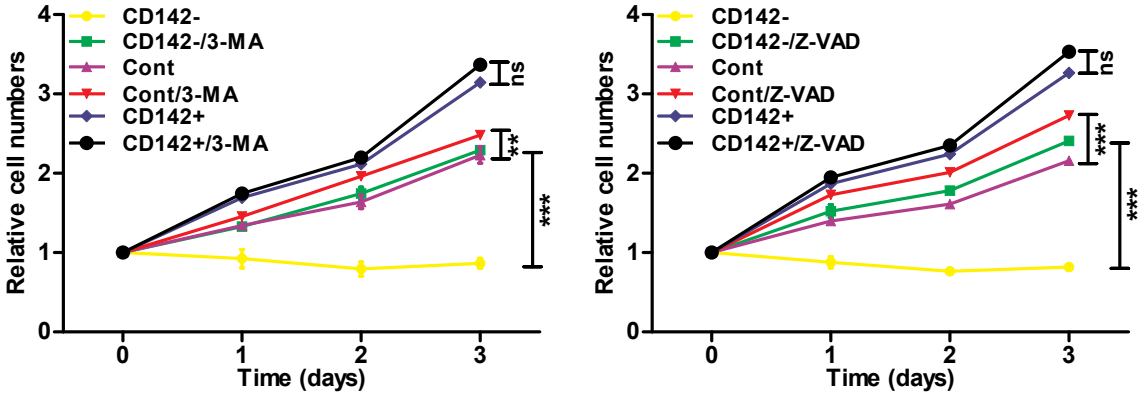

Fig. S1 Treatment with 3-MA or Z-VAD promoted the proliferation of CD142^{-} and control WiT49 cells.